

TABLE 1 Simulated Performances of Reflectarray at Different Frequencies (in Four Cases)

Frequency (GHz)	9.50	9.75	10.0	10.25	10.5	
Directivity (dBi)	Case no. 11	14.6	16.1	16.8	14.7	14.0
	Case no. 10	14.7	14.9	16.7	16.3	16.0
	Case no. 00	15.6	16.0	17.4	15.6	14.7
	Case no. 01	16.1	16.3	14.3	12.7	12.7

sample are simulated and tested in both cases of with and without EBG ground plate respectively as shown in Figure 6. The results are summarized below.

3. RESULTS WITH DISCUSSION

Table 1 lists the simulated results of directivity and back-lobe versus frequency for a 37-element reflectarray mentioned earlier, where:

Case no. 11—designed and also constructed according to a EBG of perforated ground plate,

Case no. 10—designed according to a EBG of perforated ground plate, but constructed from a solid ground plate;

Case no. 00—designed and also constructed according to a solid ground plate,

Case no. 01—designed according to a solid ground plate, but constructed from a EBG of perforated ground plate, (denote the “yes” as “1” and “no” as “0” for the digits; the first digit means if designed with EBG, and the second one means if constructed with EBG.)

The comparison between no. 00 and no. 01 seems a great difference in directivity, that means a unbalanced estimation for a reasonable design (using the left curve in Fig. 2) of normal reflectarray and an unreasonable construction with perforated plate (corresponding to the right curve in Fig. 2).

If the comparison is made between two reasonable designs of reflectarray no. 11 and no. 00, the difference becomes less, and the directivity of normal one no. 00 is higher than the EBG one no. 11 at 10 GHz, due to the cause discussed later; As shown in Figure 2 that the curve for solid plate (without EBG) is always on the right side of the curve for perforated plate (with EBG). Hence, when the design for cases no. 11 and no. 00 under the condition of same size of initial patch, and then the sizes of subsequent square patches are always different, where the patch size of no. 00 is larger than that of no. 11. Usually, the effective aperture of element is proportional to the patch size, thus the effective aperture of no. 00 is greater than that of no. 11 for each element of the reflectarray. And then the directivity of reflectarray of case no. 00 is larger than that of case no. 00 when the effective aperture of each element can really sum up without overlap over the whole aperture, which is validated by simulation of reflectarray with different initial patch size as shown in Figure 3 and by measurement results in Figure 6. If a reflectarray with EBG structure, designed in case no. 11 according to the phase curve (left) of Figure 2 is replaced its perforated ground plate by solid one (case no. 10) only, then the gain of the reflectarray becomes smaller at the designed frequency. However, it is not a measurable comparison in the gain, because the phase shift used in case no. 10 is not correct.

Obviously, the excited mechanism of reflectarray is quite different from that of general patch antenna fed by coaxial probe or microstrip line. For the patch antenna, the excited electric field within the substrate is perpendicular to the substrate; it produces the surface wave, but will be fortunately suppressed by the EBG structure. However, for the reflectarray under normal incidence, the electric field is parallel to the substrate, and then the backward Poynting vector exists as shown in Figure 4 even if a 2D EBG structure with square holes in the ground plate is employed. Figure

5 shows that with the increase of incident angle (with respect to xoy plane) from 0° to 90°, the backward Poynting vector obviously increases for both two cases of with or without EBG structure; furthermore, a switching angle about 45° transfers the relative strength of the backward Poynting vector between the cases of ground plate with and without EBG structure. So only in the case of offset feeding, the EBG structure can improve the gain of reflectarray antenna because of less backward radiation.

4. CONCLUSION

By using EBG structure into the ground plane of reflectarray, the gain cannot always be improved, only if for the case of offset feeding while the transverse surface wave can be prohibited. The theoretical discussion is given as well as the specific design samples to verify the results.

REFERENCES

1. J. Huang, Microstrip reflectarray, IEEE Intern Symp Antennas Propag London, Ontario, Canada (1991), 612–615.
2. J.A. Encinar, Design of a dual frequency reflectarray using microstrip stacked patches of variable size, Electron Lett 32 (1996).
3. D.M. Pozar and T.A. Metzler, Analysis of a reflectarray antenna using microstrip patches of variables size, Electron Lett 32 (1996), 1049–1050.
4. D.M. Pozar, S.D. Targonski, and H.D. Syrigos, Design of millimeter wave microstrip reflectarrays, IEEE Trans Antennas Propag 45 (1997), 287–296.
5. K.M. Shum, Q. Xue, C.H. Chan, and K.M. Luk, Investigation of microstrip reflectarray using a photonic bandgap structure, Microwave Opt Technol Lett 28 (2001), 114–116.
6. Z.-H. Wu, W.-X. Zhang, and Z.-G. Liu, A dual-layered wideband microstrip reflectarray antenna with variable polarization, Microwave Opt Technol Lett 48 (2006), 1429–1432.
7. V. Radisic, Y.X. Qian, R. Coccioli, and T. Itoh, Novel 2-D photonic bandgap structure for microstrip lines, IEEE Microwave Guided Wave Lett 8 (1998), 69–71.
8. Z.G. Liu and W.X. Zhang, A dual-polarized array antenna consisting of traveling wave radiators, In: Progress in Electromagnetic Research Symposium, Nanjing, 2004, p. 394.

© 2007 Wiley Periodicals, Inc.

DESIGN OF MULTI-LAYERED POLYGONAL HELIX ANTENNAS FOR RFID APPLICATIONS

Jaeyul Choo,¹ Hosung Choo,¹ Ikmo Park,² and Yisok Oh¹

¹ School of Electronics and Electrical Engineering, Hongik University, 72–1 Sangsu-dong, Mapo-gu, Seoul 121–791, Korea

² Department of Electrical and Computer Engineering, Ajou University, 5 Wonchon-dong, Youngtong-gu, Suwon 443–749, Korea

Received 15 January 2007

ABSTRACT: In this letter, we propose a novel printed helix antenna for an RFID reader in the UHF band. The printed microstrip line of the antenna is first wound outside a polygonal-shaped layer and then wound on an inner layer to control the overall gain and the radiation pattern of the antenna. On each layer, the winding pitch angles can have either negative or positive values, which results in a circularly polarized (CP) broad bandwidth. The structural details of the antenna were optimized using the Pareto genetic algorithm (GA), which allowed for excellent performance with the use of RFID reader antennas. The optimized two-layered polygonal helix was fabricated on a flexible cardboard substrate. Performances of the antenna were measured and compared with

Key words: Broad bandwidth, broad CP bandwidth, reader antenna, RFID

1. INTRODUCTION

In recent years, there has been an increased interest in radio frequency identification (RFID) as an automatic identification tool that is superior to bar codes and infrared technology. An RFID reader identifies a tag by extracting information from weak scattered radio frequency signals, and as such, it requires an antenna with a very low return loss and a high efficiency over a broad bandwidth. In addition, the radiation pattern of the antenna should be suitable to achieve the appropriate readable range for a given application. Moreover, a high quality of circular polarization (CP) is needed over a wide frequency range to extend the readable range of the system [1, 2]. Helix antennas, because of their small profiles, high gains, and suitable CP characteristics, have recently been investigated for use in a variety of wireless applications [3–5]. Conventional helix antennas, however, do not fully and simultaneously satisfy the aforementioned characteristics required for RFID application. Moreover, little research on the application of helical structures to RFID reader antennas has been conducted.

In this letter, we propose a novel multi-layered polygonal helix antenna (MPHA) for RFID reader applications that works in the UHF band (860–960 MHz). The printed microstrip line of the MPHA is first wound outside the polygonal-shaped layer and then on the inner layer to achieve control of the overall gain and the radiation pattern. On each layer, the wound printed microstrip line can have either negative or positive pitch angle values. This allows for easy control of the phase of the current on the microstrip line and, as a result, leads to desired CP characteristics. Detailed design parameters, such as the number of layers, the bending angles of each layer, and the pitch angles of the microstrip line on each layer

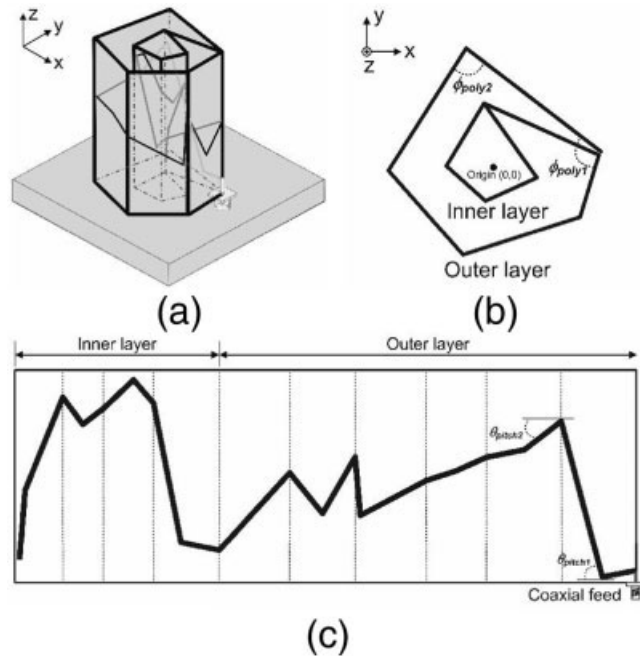


Figure 1 Configuration of the two-layered MPHA: (a) perspective view of the MPHA. (b) top view of the MPHA. (c) unfolded structure of the MPHA.

Table 1 Design Parameters for the MPHA

Bend Point		Position (mm)		
		x	y	Z
Outer layer	Startpoint	55	0	0
	1	55	0	7
	2	27	25	1
	3	-7	55	127
	4	-27	27	93
	5	-54	-10	87
	6	-34	-36	75
	7	-25	-39	69
	8	28	-46	55
	9	31	-46	94
Inner layer	10	42	-25	52
	11	55	0	84
	12	-3	24	24
	13	-12	10	30
	14	-23	-6	130
	15	-14	-13	159
	16	-2	-24	125
	17	7	-19	115
	18	21	-12	128
	19	5	12	78
	Endpoint	-3	24	17

are then determined using the Numerical Electromagnetic Code (NEC) in conjunction with the Pareto genetic algorithm (GA) [6]. Optimal designs showed superior performances as measured in terms of matching bandwidth ($S_{11} < -10$ dB), CP bandwidth (axial ratio < 3 dB), readable range, and antenna gain. To verify the GA result, an optimized two-layered polygonal helix was fabricated on a flexible substrate, and its performances were measured and compared with those of simulations.

2. ANTENNA GEOMETRY AND GA OPTIMIZATION

The proposed MPHA structure, which is constructed with two layered polygons for operation at 912 MHz, is shown in Figure 1. The microstrip line on the MPHA is first wound outside the polygonal layer and then on the inner layer. The inner angles of each layer are bent to $\{\phi_{poly1}, \phi_{poly2}, \dots, \phi_{polyN}\}$, as shown in Figure 1(b), and the microstrip lines on each layer are printed at pitch angles of $\{\theta_{pitch1}, \theta_{pitch2}, \dots, \theta_{pitchN}\}$, as shown in Figure 1(c). The overall gain and the radiation pattern of the MPHA are primarily controlled by the polygon's inner angles ϕ_{poly} and the

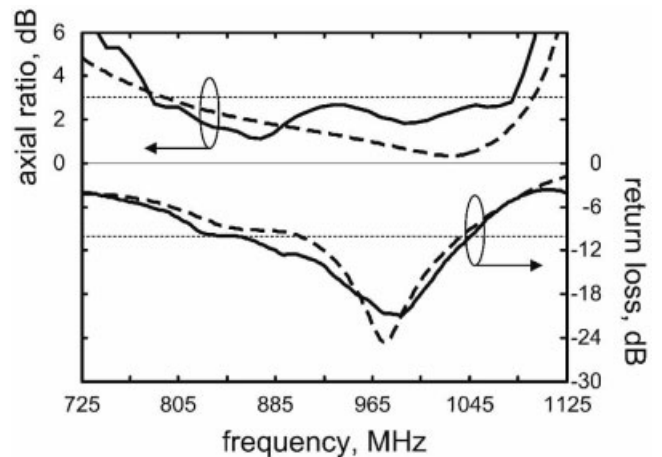


Figure 2 Return loss and axial ratio of the MPHA

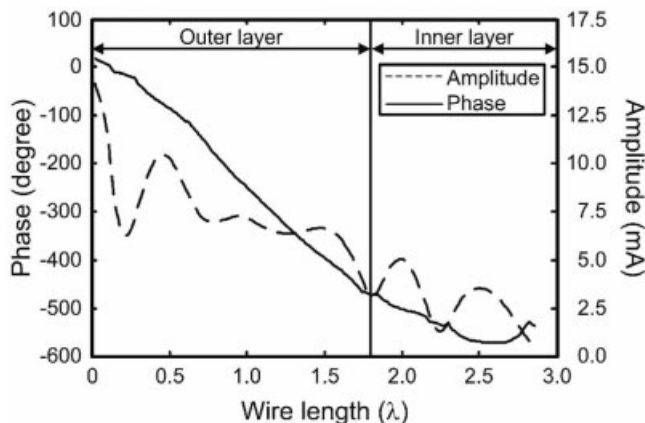


Figure 3 Current distribution on the microstrip line.

number of layers N_L . Meanwhile, the polygon's pitch angles θ_{pitch} determine the distribution of the induced current of the microstrip line of each layer, which allows for low return loss and broad CP radiation characteristics. The MPHA can be easily built from a printed microstrip line structure by folding the substrate along the dashed lines shown in Figure 1(c).

To determine the required design parameters of the given structure, the Pareto GA was used with a NEC simulator [6, 7]. The four design goals guiding the Pareto GA optimization were: the maximum matching bandwidth with highest efficiency, the broadest CP bandwidth, an optimal readable range and a small antenna size. In applying this process, the GA optimization is mainly decided by cost functions based on the design goals. The four cost functions used in the GA optimization were defined as:

$$\text{Cost 1} = \frac{1}{2} \left(1 - \frac{\text{Eff}_{\text{Reader}} \times \text{BW}_{\text{Reader}}}{\text{BW}_{\text{RFID}}} \right) + \text{RQ} \quad (1)$$

Where

$$\text{RQ} = \begin{cases} 0 & \text{if } \text{Eff}_{\text{Reader}} \times \text{BW}_{\text{Reader}} < \text{BW}_{\text{RFID}} \\ \max \{ \text{return loss} \} & \text{if } \text{Eff}_{\text{Reader}} \times \text{BW}_{\text{Reader}} > \text{BW}_{\text{RFID}} \end{cases}$$

$$\text{Cost 2} = \frac{1}{2} \left(1 - \frac{\text{CPBW}_{\text{Reader}}}{\text{BW}_{\text{RFID}}} \right) + \text{AQ} \quad (2)$$

$$\text{Where } \text{AQ} = \begin{cases} 0 & \text{if } \text{CPBW}_{\text{Reader}} < \text{BW}_{\text{RFID}} \\ \max \{ \text{axial ratio} \} & \text{if } \text{CPBW}_{\text{Reader}} > \text{BW}_{\text{RFID}} \end{cases}$$

$$\text{Cost 3} = \text{Size}_{\text{Norm}} \quad (3)$$

$$\text{Cost 4} = 1 - \frac{\text{RR}_{\text{Reader}}}{\text{RR}_{\text{RFID}}} \quad (4)$$

Cost 1 was computed as the product of the efficiency ($\text{Eff}_{\text{Reader}}$) and the matching bandwidth ($\text{BW}_{\text{Reader}}$) of the sample antenna normalized with respect to the BW_{RFID} (860–960 MHz), which is the bandwidth required for RFID in the UHF band. In addition, the return loss quality (RQ) was used to minimize the maximum return loss value within the BW_{RFID} when the $\text{Eff}_{\text{Reader}} \times \text{BW}_{\text{Reader}}$ exceeded the BW_{RFID} . Cost 2 was calculated by taking into account the comparison between the $\text{CPBW}_{\text{Reader}}$ and the BW_{RFID} as well as the axial ratio quality (AQ) to minimize the maximum axial ratio. Cost 3 was defined as the radius r of the smallest circle that encloses the entire antenna structure. Cost 4 was defined in terms of the ratio of the readable range ($\text{RR}_{\text{Reader}}$) of the sample antenna to the required readable range (RR_{RFID}). The readable range was derived from the radar detectable range equation [1]. The optimized design parameters associated with the four cost functions can be found after a convergence of the Pareto GA process.

3. RESULTS

Optimized antennas resulting from the GA process exhibited broad matching and CP bandwidths. In addition, some of the optimized designs showed an antenna gain nearly equal to the maximum gain achievable by a multi-layered antenna (based on the fundamental gain limits [8]). These high gain and broad bandwidth characteristics led to the design of the MPHA with a readable range suitable for the intended RFID application. To experimentally verify the optimized designs, a sample antenna was fabricated with a two-layered structure of $kr = 3.2$ on a 20 cm \times 20 cm ground plane, where k is the wave number at 912 MHz and r is the radius of the sphere that encloses the entire antenna structure. Table 1 shows the geometric bend points of the sample antenna which consists of a pentagonal outer layer and a quadrangular inner layer. The antenna was built by folding a flexible cardboard ($\epsilon_r = 2.3$, $\tan\delta = 0.022$, thickness = 2 mm) with copper tape (width = 2 mm). The base of the folded cardboard was inserted into Styrofoam board to fix the

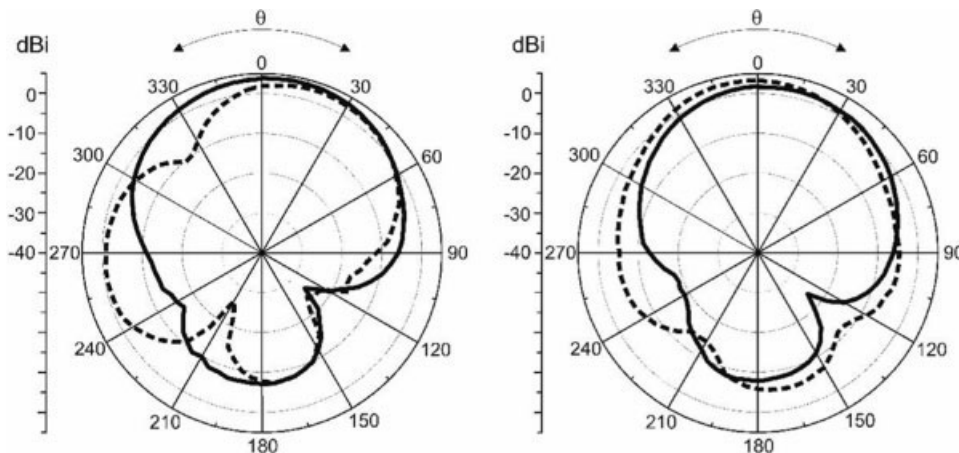


Figure 4 Measured radiation patterns of the MPHA at 912 MHz; (a) x - z plane, (b) y - z plane.

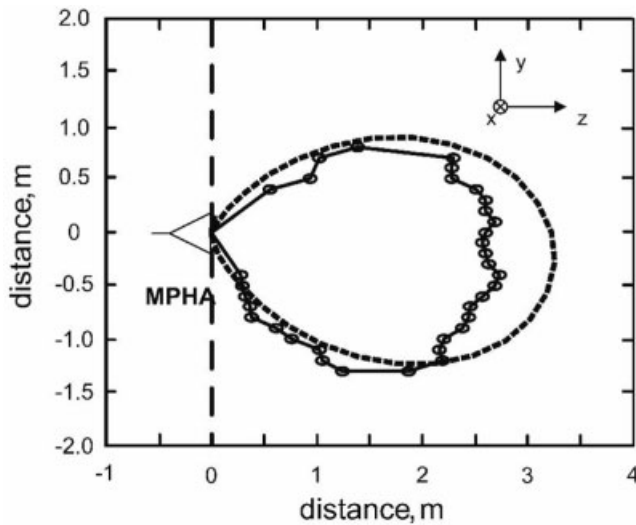


Figure 5 Readable zone of the MPHA

inner angles of the polygons, and then the antenna was fed via a coaxial probe with a characteristic impedance of 50Ω .

Figure 2 shows the measured and simulated return loss and axial ratio of the fabricated MPHA discussed above. The measured matching bandwidth ($S_{11} < -10$ dB) of 21.4% (850–1045 MHz) was slightly broader than the simulated bandwidth of 15.8% (904–1038 MHz). The measured CP bandwidth (axial ratio < 3 dB) of 31.9% (780–1071 MHz) was quite similar to the simulated CP bandwidth of 33.2% (794–1097 MHz). The efficiency of the fabricated antenna was measured using the Wheeler cap method, which yielded a value of about 91% on the operating frequency band [9].

To interpret the characteristics of the fabricated antenna, the amplitude and the phase of the induced current on the antenna body were analyzed at 912 MHz, as shown in Figure 3. The phase of the current on the outside layer decayed in a nearly linear fashion, forming the traveling wave on the printed microstrip line. This traveling wave apparently allowed the broadband CP bandwidth in excess of 30% in the broadside direction. This quasi-linear phase on the current is made possible by allowing the pitch angle (θ_{pitch}) to assume either negative or positive values. When only positive pitch angle values were used, the resulting performance did not lead to broad CP bandwidth. Figure 4 shows the measured radiation pattern of the fabricated antenna at 912 MHz. Although the antenna has some back lobe owing to the finite-size ground plane, the results show that the antenna radiates with a total power gain of about 6 dBi in the broadside direction ($G_{\theta} \approx 3$ dBi, $G_{\phi} \approx 3$ dBi).

The readable range of the proposed antenna was measured using an ALR-2850 reader and an ALL-9238 tag [10], as shown in Figure 5. The solid line represents the measured readable zone and the dashed line, which was calculated using (5), is the detectable range of the test radar system [1].

$$R_{\text{Max}} = \sqrt[4]{\frac{P_T (G_{\text{Tag}})^2 (G_{\text{Reader}})^2}{P_{R,\text{min}}} \left(\frac{\lambda}{4\pi}\right)^4} \quad (5)$$

Here P_T is 1 W of power radiated by the reader, G_{Tag} is the radiation pattern of the tag that is similar to a half wavelength dipole, G_{reader} is the gain of the MPHA, and $P_{R,\text{min}}$ is -50 dBm of the minimum power detectable by the reader. As can be seen in (5), the maximum readable range is proportional to the square root of the gain of the antenna. The measured readable zone shows good agreement with the simulated result except for the slightly shorter range in the broadside

direction. This comparison, along with the previously presented results, confirms that the proposed MPHA possesses excellent characteristics as a reader antenna with stable readability.

4. CONCLUSION

An RFID reader antenna for operation in the UHF band was investigated, and a new helix antenna called the MPHA was proposed. To satisfy the characteristics required for an RFID reader antenna, the structural details of the MPHA were optimized using the Pareto GA. The number and the shape of the polygonal layers were found to be critical design parameters in controlling the gain and the radiation pattern of the antenna. The variable pitch angles of the printed microstrip line allowed the phase of the induced current to linearly decrease along the microstrip line, which helped to achieve broadband CP characteristics in the broadside direction. The antenna based on the optimal design was built of a copper microstrip line on flexible cardboard, and it showed a matching bandwidth of 21.4% ($S_{11} < -10$ dB), a CP bandwidth of 31.9% (axial ratio < 3 dB), and a readable zone of 5 m^2 with $kr = 3.2$.

ACKNOWLEDGMENT

This research is supported by Seoul R&BD program in Korea.

REFERENCES

1. K. Finkenzeller, RFID handbook, 2nd ed., Wiley, West Sussex, England, 2003.
2. W. Rankl and W. Effing, Smart card handbook, Wiley, New York, 2003.
3. H.E. King and J.L. Wong, Characteristics of 1 to 8 wavelength uniform helical antennas, IEEE Trans Antennas Propagat 28 (1980), 291–296.
4. A. Safaai-Jazi and J.C. Cardoso, Radiation characteristics of a spherical helical antenna, IEE Proc Microwave Antennas Propagat 143 (1996), 7–12.
5. J.M. Tranquilla and S.R. Best, A study of the quadrifilar helix antenna for global positioning system applications, IEEE Trans Antennas Propagat 38 (1990), 1545–1550.
6. D. Goldberg, Genetic algorithms in search, optimization and machine learning, Addison Wesley, Reading, MA, 1989.
7. J.H. Jung, H. Choo, and I. Park, Small broadband disc-loaded monopole antenna with probe feed and folded stripline, Electron Lett 41 (2005), 788–799.
8. R. Harrington, On the gain and beamwidth of directional antennas, IEEE Trans Antennas Propagat 6 (1958), 219–225.
9. H. Choo, R. Rogers, and H. Ling, On the Wheeler cap method for measuring the efficiency of microstrip antennas, IEEE Trans Antennas Propagat 53 (2005), 2328–2332.
10. RFID system. Available at <http://www.alientechnology.com>

© 2007 Wiley Periodicals, Inc.